Aerosol Science and Technology
Publication details, including instructions for authors and subscription information:
http://www.tandfonline.com/loi/uast20

A Transition from Heterogeneous to Homogeneous Nucleation in the Turbulent Mixing CNC

Rashid Mavliev , Philip K. Hopke , Hwa-Chi Wang & Doh-Won Lee
Published online: 30 Nov 2010.

To cite this article: Rashid Mavliev , Philip K. Hopke , Hwa-Chi Wang & Doh-Won Lee (2001) A Transition from Heterogeneous to Homogeneous Nucleation in the Turbulent Mixing CNC, Aerosol Science and Technology, 35:1, 586-595

To link to this article: http://dx.doi.org/10.1080/02786820119393

Aerosol Science and Technology 35: 586–595 (2001)

Published by Taylor and Francis
0278-6826/01/$12.00 + .00

A Transition from Heterogeneous to Homogeneous Nucleation in the Turbulent Mixing CNC

Rashid Mavliev,[1] Philip K. Hopke,[2] Hwa-Chi Wang,[1,3] and Doh-Won Lee[2]
[1]*Illinois Institute of Technology, Chicago, Illinois*
[2]*Clarkson University, Potsdam, New York*
[3]*Air Liquide, Chicago Research Center, Countryside, Illinois*

A new method for changing the supersaturation in the Turbulent Mixing CNC has been developed and used to examine the transition from heterogeneous nucleation of test particles to homogenous nucleation of working fluid: dibutylphthlate (DBP). Supersaturation was controlled by changing the DBP vapor pressure in the nozzle flow by saturating only a predetermined part of the flow, while the total flow and temperature remain constant. This approach allows for the changing of the initial DBP vapor pressure, while keeping the flow structure and temperature field unchanged. The DBP concentration in the outlet of the vapor generator was measured experimentally for different ratios of saturated and bypass flows and found to be close to estimated values. Experimental results for transitions from heterogeneous nucleation to homogeneous nucleation are presented for NaCl and WO_x particles at various DBP vapor pressures. With an increasing of the DBP vapor pressure, the concentration of enlarged particles increases until it reaches a plateau. At higher initial values of DBP pressure, homogeneous nucleation prevails, and the number concentration of particles follows a curve typical for homogeneous nucleation recorded in the absence of nuclei. Nuclei with different mobility diameters were activated at different values of vapor pressure. There are significant differences in the slopes of particle activation curves for NaCl and WO_x particles. The reasons for such differences are a subject for continuing research.

INTRODUCTION

Recently, in the field of nanometer-sized particles, attention has been paid to homogeneous nucleation, binary nucleation, ion-induced nucleation, and simultaneous heterogeneous and homogeneous nucleation because of the importance of these processes in atmospheric particle formation (Kim et al. 1998). In addition, discrepancies between theory and experiment have stimulated new research in this field. Several new techniques have been developed for more accurately characterizing heavy ions and particles in the nanometer-size range.

The Condensation Nuclei Counter (CNC), which grows primary particles (nuclei) up to a more easily detectable size, is one of the most widely used devices for studying particles below 0.1 μm. A general description of a CNC is given in many books and reviews (for example, Willeke and Baron (1993)). Several types of CNCs are used in aerosol research. The main difference among these CNC designs is the way they produce supersaturation that leads to particle growth up to a predetermined size for subsequent detection. In an expansion-type CNC, supersaturation is generated by adiabatic cooling during pressure reduction. It is a batch instrument and has been used in atmospheric aerosol research for many years. A continuous CNC (Agarwal and Sem 1980) is widely used today. Supersaturation is formed by cooling the laminar aerosol flow that was saturated with working fluid vapor. The third type of CNC is based on turbulent mixing of the flows with particles and working fluid vapor. This type of instrument has not yet been commercialized. It was described first by Kogan and Burnashova (1960) and was further developed in different versions by Okuyama et al. (1984), Ankilov et al. (1991), Kousaka (1993), and Mavliev and Wang (2000). The major advantage of the turbulent mixing CNC (TMCNC) is the flexibility of generating supersaturation by simply mixing the aerosol flow and a flow saturated with the working fluid vapor.

The CNC is one of the most sensitive methods for detecting nanometer particles. The detection limit can reach 2–3 nm (Stolzenburg and McMurry 1991; McDermont et al. 1991; Okuyama et al. 1984; Mavliev and Wang 2000). The minimum detection efficiency of CNCs is very sensitive to the size of particles (Makela et al. 1996).

Although a CNC is primarily devoted to measuring the number concentration of particles, in recent years it has been shown that a CNC can be used to measure the size distribution of nanometer particles. The size distribution of nuclei can be measured by means of changing the CNC's sensitivity (McDermont

Received 29 November 1999; accepted 11 May 2000.
Address correspondence to Philip K. Hopke, Department of Chemistry, Clarkson University, Box 5705, Potsdam, NY 13699-5705. E-mail: hopkepk@clarkson.edu

Table 1
Effect of particle charge on estimated Kelvin diameter

d_{kelv} with charge	1.50	1.60	1.70	1.80	1.90	2.00	2.20	2.40	2.60	3.00
d_{kelv} without charge	2.08	2.08	2.10	2.15	2.20	2.27	2.41	2.58	2.75	3.11

et al. 1991) and by means of measuring the size of grown particles (Ahn and Liu 1990; Rebours et al. 1996; Saros et al. 1996). The last approach is based on the fact that the growth of smaller particles is delayed because of the Kelvin effect that results in the final size of particles being dependent on initial nucleus size. However, size resolution is not satisfactory and operational range is limited to a range of 3–10 nm. In addition, the growth time for particles of the same size depends strongly on spatial uniformity of supersaturation. For most continuous flow CNC's, the spatial distribution of supersaturation is not uniform because of the use of diffusive cooling in the laminar flow (Stolzenburg 1988).

In the present article, a new approach for changing the TMCNC sensitivity is described. The approach is based on changing the vapor pressure of working fluid by changing the ratio of saturated and by-pass flows in the vapor generator. This approach was used to investigate the transition from heterogeneous to homogeneous nucleation for two types of initial nuclei.

APPROACH

Basics of Heterogeneous Nucleation

It is well known that particles start to grow when subjected to sufficiently supersaturated vapor conditions. This phenomenon is known as heterogeneous nucleation and is the working principle for the widely used CNC. In a CNC, particles are allowed to grow to sufficient size for further detection. The relationship between vapor pressure and particle diameter when the process of condensation starts to prevail over evaporation is

$$\ln S = \frac{4M}{\rho RT}\frac{\sigma}{d_{kelv}}, \qquad [1]$$

where d_{kelv} is the Kelvin diameter, σ is surface tension, M is molecular weight, ρ is density of liquid, R is the universal gas constant, and the supersaturation $S = P/P_{sat}(T)$. $P_{sat}(T)$ is the saturation vapor pressure at temperature T. At a given S value, particles greater than the Kelvin diameter are activated and followed by condensational growth. Particles smaller than the Kelvin diameter are not activated and eventually evaporate.

If particles carry an electric charge, the evaporation/condensation equilibrium condition is affected. The supersaturation required for droplet growth in this case can be expressed as

$$\ln S = \frac{4M}{\rho Rt}\left(\frac{\sigma}{d_{kelv}} - \frac{q^2(1-1/\varepsilon)}{2\pi^2 d_{kelv}^4 \varepsilon_0}\right), \qquad [2]$$

where q is the electrostatic charge and ε and ε_0 are dielectric constants of the droplet and vacuum, respectively (Scheibel and Porstendörfer 1986). The charge effect is shown in Table 1, where estimated Kelvin diameters are compared for particles with charge and without charge. Charge effects on nucleation are negligible for particles above 3 nm. However, for smaller particles, it could be substantial and should be taken into account.

Effects of Nuclei Origin

The interaction between the nuclei and vapor molecules has a strong influence on the heterogeneous nucleation process. Equations (1) and (2) that relate the Kelvin diameter to the supersaturation ratio are simplified cases of heterogeneous nucleation. In reality, the interaction between the vapor and particles is not well defined, especially for atmospheric aerosols of unknown origin.

If the nucleating particle is not perfectly wettable by the working fluid, the situation becomes more complicated. The formation energy of the working fluid embryo will involve the interaction of solid-liquid and liquid-gas interfaces. According to Fletcher (1969), one of the most important parameters in this case is the contact angle between the particle surface and the condensed phase. However, the contact angle on nanometer-size particles is not known and the contact angle of bulk material may not be valid. Experimental investigation of the effects of the nuclei substance on nucleation activation becomes extremely important. Nevertheless, only a few publications are available in the literature.

Helsper and Neissner (1985) investigated the effect of the vapor substance on the behavior of an expansion-type CNC for two working fluids, water and butanol. They found that particle substance (Ag and NaCl) did not affect the Kelvin diameter when butanol was used as the working fluid. However, the size of NaCl particles was overestimated by 2.5 times when water was used. Similar results were found by Porstendorfer et al. (1985). Kesten et al. (1991) found different detection efficiency of the TSI CNC 3025 with butanol as a working fluid for NaCl and Ag particles. Kousaka et al. (1984) found less profound but still different results for NaCl and Ag particles. The brief description of results by Madelaine and Metayer (1980) showed an essential difference of CNC sensitivity for NaCl, V_2O_5, and H_2SO_4 particles. These initial reports suggest the influence of nucleus origin and working fluid vapor. However, there is insufficient

data for establishing a complete theoretical description of the phenomena.

Formation of the Supersaturation by Turbulent Mixing

In the TMCNC, the aerosol flow ("cold" flow, Q_a) is mixed with the gas flow saturated with the vapor of a working fluid ("hot" flow, Q_v). The mixing of "cold" and "hot" flows causes the supersaturation of the working fluid vapor because of the immediate temperature decrease of the mixed flow. As a result, particles greater than the equivalent Kelvin diameter will start to grow. In our system, the initial "hot" flow can be considered as a turbulent jet in a confined space. According to Abramovich (1963), the spatial structure of a jet in a confined space is similar to that of a free jet. The temperature and pressure fields are then described by

$$\begin{aligned} T &= T_1 + (T_2 - T_1)n, \\ P &= P_1 + (P_2 - P_1)n, \end{aligned} \qquad [3]$$

where the local mixing ratio n is a function of the jet coordinates and indices 1 and 2 correspond to the "cold" and "hot" components, respectively. This simplified approach is valid for low vapor concentration, and the thermodynamic parameters of the mixture of these two flows are practically the same as those in the absence of vapor. The mixing ratio changes from 0 at the jet boundary to 1 at the center of the jet, immediately downstream of the nozzle. The flow farther away from the nozzle can be considered uniform. The transition from a jet to a uniform flow occurs at the distance from the nozzle where the axial velocity is close to the average velocity of the flow. The final value of the mixing ratio is

$$n_{fin} = \frac{Q_v}{(Q_v + Q_a)}, \qquad [4]$$

where n_{fin} is equal to parameter R_h used for estimations by Okuyama et al. (1984). Instead of numerically solving the fluid dynamic equations, a simple approach can be employed by treating the mixing ratio as an independent variable in order to examine the impact of various designs and operating parameters. For a given mixing ratio, the local values of supersaturation $S = P/P_{sat}(T)$, the corresponding Kelvin diameter, and the homogeneous nucleation rate can be determined. Calculations were performed using the Excel spreadsheet program. The Calculating procedure consists of the following:

- generating a set of n values in the range of 0.02–200,
- calculating local temperature and pressure values for each value of n using Equation (3),
- calculating saturated pressure and surface tension values at the temperature corresponding to value n,
- calculating supersaturation and Kelvin diameter values, and
- calculating the homogeneous nucleation rate using previously determined parameters.

Experimental Setup

The experimental system is shown schematically in Figure 1. The basic components are the particle generators, the Differential Mobility Analyzer (DMA), and the CNCs. The TMCNC employed was essentially the same as that described previously (Mavliev and Wang 2000), except for the vapor generator. A more detailed description will be given in the following sections. A subset of this set up was used in previous experiments on the detection efficiency evaluation of a turbulent mixing CNC at high flow rates.

Particle Generation

Two different types of particles were used in the experiments. Particles of NaCl were generated by evaporation in a high temperature furnace and subsequently cooled off the vapor by mixing it with a cold flow. This method allows particle generation in the size range of 2–20 nm. Test particles of WO_x were generated by a hot wire method similar to that described by Reischl et al. (1997). Tungsten wire (Aldrich) was heated by electric current inside a glass tube with a filtered airflow of 3 lpm. Particle size and number concentration were controlled by varying the heating power. The flow pattern was arranged to allow a quick change from NaCl to WO_x particles without disturbing the DMA and CNC operating parameters. This flexibility allowed for the investigation of heterogeneous nucleation for both substances under very similar conditions.

The nucleation activity of the particles depends strongly on their size. The monodisperse fraction of particles was obtained from the original polydisperse distribution by the Vienna-type DMA ($Qsh = 28$ lpm, $Qs = 3$ lpm) and directed to the Faraday Cup Electrometer (FCE) ($Q1 = 2.5$ lpm) and to the TMCNC ($Q2 = 0.5$ lpm). At a short distance from the flow split, the CNC flow was diluted with filtered air of 1.5 lpm providing the total sample flow of 2 lpm. The dilution airflow was pushed through a heat exchanger cooled by water from the circulating bath at a temperature of 20°C. Diffusion losses of particles in the connection line between the DMA outlet and the CNC inlet (total length 0.55 m) were estimated using well-known formulas for particle penetration through cylindrical tubes (Willeke and Baron 1993). Estimated diffusion losses can reach 45% for 2 nm particles; for bigger particles, diffusion losses become lower with 20% for 4 nm and 10% for 10 nm particles. Additional particle losses that could occur in the entrance of the CNC system are negligible according to our estimations.

The Vienna-type DMA (HAUKE, Vienna, Austria) is a suitable instrument for particle separation in a size range below 50 nm (Fissan et al. 1996). Recent research on selection efficiency shows that proper adjustment of the sample/sheath flow ratio allows an attainment of 5% resolution at the high end and 10% at the low end for sizes ~1 nm (Rossel-Lompart et al. 1996). At sample and sheath flow ratios used in the experiments, the width of the transfer function should be approximately 12%, but because of the effect of diffusion broadening in the small

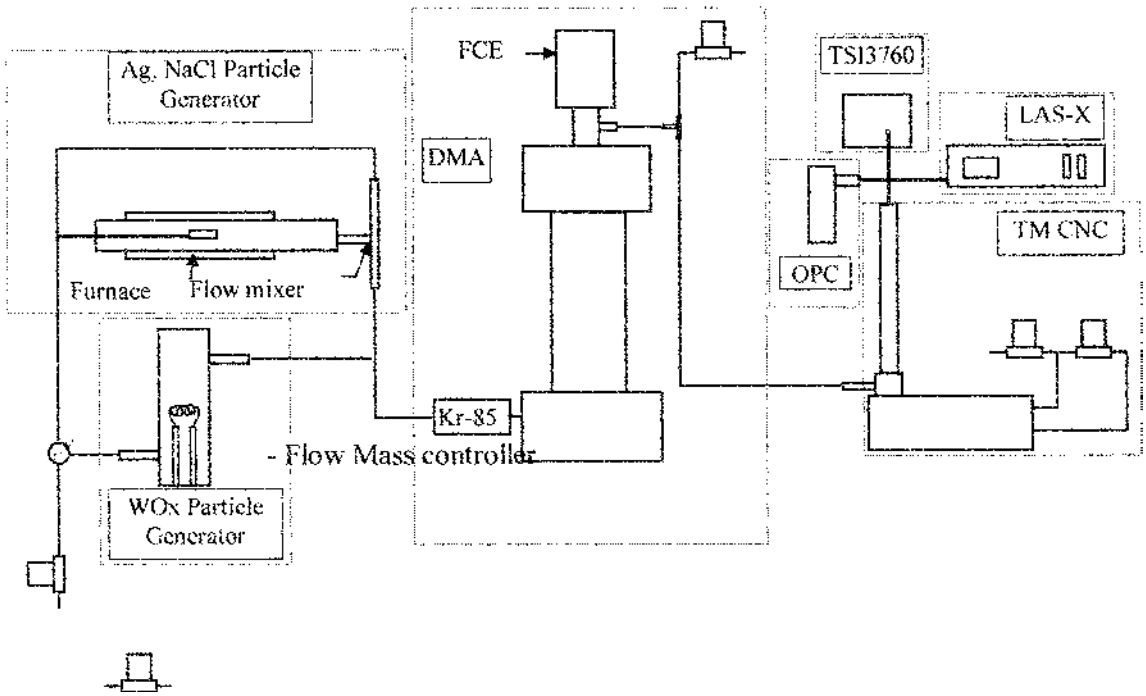

Figure 1. Schematic diagram of the experimental set up. Vienna-type DMA, FCE, TMCNC, Laser Aerosol Spectrometer (PMS LAS-X), Optical Particle Counter OPC-501 (PMS, OPC), TSI Condensation Nuclei Counter (TSI 3760), and Aerosol Charger Kr-85 (TSI).

particle range, the real width can reach 20% (Stolzenburg 1988; Reischl et al. 1997).

CNC Operation Principle

The scheme of the TMCNC is shown in Figure 2. In TMCNC, the aerosol flow ("cold" flow) mixed with the gas flow saturated by working fluid vapor ("hot" flow). The mixing of "cold" and "hot" flows causes supersaturation because the saturation pressure corresponding to the system temperature after mixing is lower than the vapor pressure in the mixed flow. Flows (at least one) should be turbulent to provide quick mixing. The common technique to vary the degree of supersaturation in a TMCNC is to adjust the temperature of the vapor generator and therefore the equivalent Kelvin diameter. A disadvantage of this method is that the temperature of the mixing zone depends on the temperature of the vapor generator and therefore the effect of supersaturation is convoluted with that of the temperature field in the mixing zone (Adachi et al. 1992). In the present research, we used another approach as described below to control supersaturation without changing the saturator temperature and flow rate and thus preserving the temperature and flow field.

The vapor generator is machined from a block of aluminum alloy that is coated with aluminum oxide (thickness $\sim 100 \mu$m). The flow channels are machined by drilling through the aluminum block. Additional holes are drilled to install the heating elements and a solid-state temperature sensor. This approach allows uniform temperature distribution within the block. The vapor generator is placed in an outer Teflon shell for insulation up to 150°C. Temperature is controlled by a circuit board with an accuracy of $\pm$ 0.1°C. Two chambers of equal size, which can be filled with a working fluid of 15–20 cm^3 by volume, are also machined. Flows from these two chambers are connected and mixed before passage to the growth tube. One of the chambers ("bottom") is partially filled with the working fluid dibutylphthalate (DBP), while the other chamber ("top") is kept dry. The degree of supersaturation is adjusted by varying the ratio of flows passing through these two chambers, which are equilibrated at the same temperature.

The saturated vapor flow is directed to a mixing chamber through a 1 mm diameter nozzle. The aerosol flow is directed into the mixing chamber through a circular opening which is formed by the nozzle and a plastic insert (see Figure 2). The main purpose of the insert (minimal opening 4 mm, total length 40 mm) is to reduce the "dead" space and the recirculation of the flow. These two coaxial flows are mixed and directed to a condensation tube downstream. A condensation tube is made of a stainless steel tube with an internal diameter of 20 mm and a length of 200 mm. The residence time of particles in the condensation tube is about 2 s, assuming a fully developed flow. The actual residence time may be somewhat shorter because of the turbulent jet flow structure at the entrance of the growth tube. However, it is sufficient for particle growth if the saturator temperature is set at 110°C or above (Mavliev and Wang 2000). The growth tube is cooled by a heat exchanger (copper tube) with water flow from a circulating bath at a temperature of 20°C to prevent the condensation of DBP vapor on optical elements downstream.

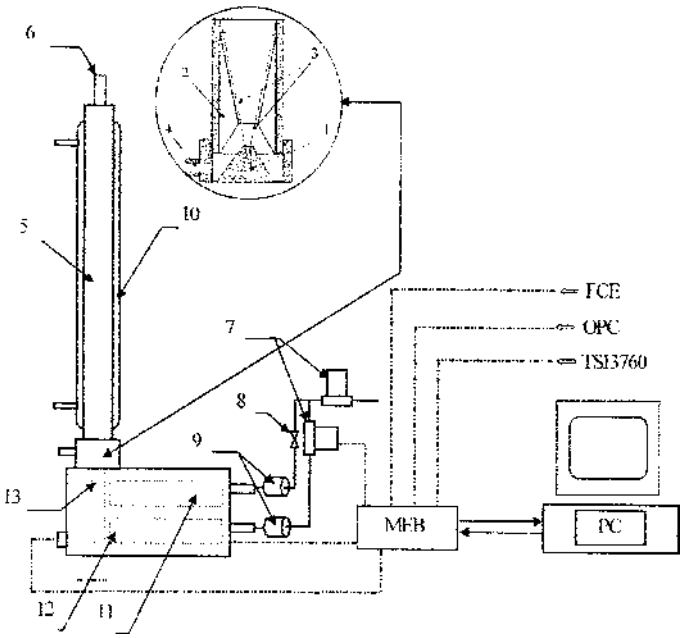

Figure 2. Scheme of TMCNC. Nozzle (1), flow compressor (2), boundary of jet (3), "cold" flow with particles (4), growth tube (5), outlet of grown particles (6), flow control system (7), critical orifice (8), aerosol filter (9), growth tube temperature control (10), "top" volume of the vapor generator (11), "bottom" volume of the vapor generator (12), flow mixer (13), and main electronic board (MEB). Solid lines are the gas flow connections; dotted lines are electrical connections.

The concentration of particles after condensation growth is measured using three particle counters: a CNC (TSI 3760), an optical particle counter (PMS OPC-501), and a laser aerosol spectrometer (PMS LAS-X). The optical counter (OPC-501) has a detection range of 0.5 μ and 5 μ and is designed for a flow rate of 2.8 lpm. The laser aerosol spectrometer (LAS-X) has four measuring ranges with detection limits of 1.5 μm, 0.3 μm, 0.17 μm, and 0.12 μm, respectively. Because the size distribution of grown particles usually did not fit in a single measuring range, the scanning mode of the LAS-X was used. This operational mode increases the time necessary to measure one size distribution to 40 s, but provides detailed size distribution of grown particles. The third instrument used to measure number concentration of grown particles, TSI CNC model 3760, has a detection limit of 14 nm and was used at a standard flow rate of 1.5 lpm. The detection limit (50% detection efficiency) of a prototype TMCNC is approximately 2.7 nm for flow rates from 1 to 2.8 lpm (Ankilov et al. 1994; Mavliev and Wang 2000).

Supersaturation Scanning

As was shown above, the activation of particle growth and CNC detection limits depend on supersaturation. The increase of supersaturation allows starting heterogeneous nucleation for smaller particles and lowering the detection limit. As supersaturation increases to a certain level, homogeneous nucleation starts to compete with heterogeneous nucleation. Therefore homogeneous nucleation is the terminal limiting factor for this method since the operating conditions have to avoid the initiation of homogeneous nucleation. Important questions are how far from this point should conditions be set and what criteria can be used to choose the operating parameters.

These criteria can be determined by scanning the supersaturation over the range of values up to the onset of homogeneous nucleation. Scaling parameters can be applied to obtain proper working conditions. Homogeneous nucleation causes a very characteristic exponential growth in particle number and can be easily identified. The onset point of homogeneous nucleation can be used to determine the supersaturation value and the corresponding Kelvin diameter under the specific working conditions.

Supersaturation scanning in the TMCNC is achieved by changing the initial vapor pressure of DBP in the "hot" flow. The carrier gas to the vapor generator (0.8 lpm) is split into two flows at the entrance. One fraction of flow is directed to the vapor generator chamber containing DBP ("bottom") and saturated with DBP vapor. Another part of the vapor generator flow is directed to the chamber without DBP ("top") but equilibrated at the same temperature. These two flows are recombined inside the vapor generator before being directed to the nozzle. This approach permits changing the initial DBP vapor pressure in the vapor generator flow by changing the ratio of flows through "top" and "bottom" chambers while keeping the flow structure and the temperature field unchanged.

The DBP concentration in the outlet of the vapor generator was measured gravimetrically. Porous metal cups were placed in the air stream at the nozzle outlet. The weight of the cups was measured before and after exposure. The DBP accumulation is directly proportional to the exposure time, indicating that the measurement procedure is correct. To measure the penetration of vapor through the porous cups, two cups are placed sequentially. The DBP amount on the second cup is negligible, indicating complete condensation of vapor on the first cup.

Experiments were performed for vapor generator flows of 0.8 and 1.6 lpm (no "cold" flow was used) and for temperatures of 115, 120, and 130°C. The measurement results for a vapor generator flow rate of 0.8 lpm and saturator temperatures of 120°C are presented in Figure 3 for different ratios of vapor flow to total flow. The dotted lines represent estimations based on saturated vapor pressure, and the symbols are experimental values. The mass of accumulated vapor substance m was estimated using the gas law:

$$m = \frac{PVM}{RT}, \qquad [5]$$

where $P_{sat}(T)$ is saturated vapor pressure, V is volume of air stream (L), M is molecular weight of DBP (278.35g/mol), R

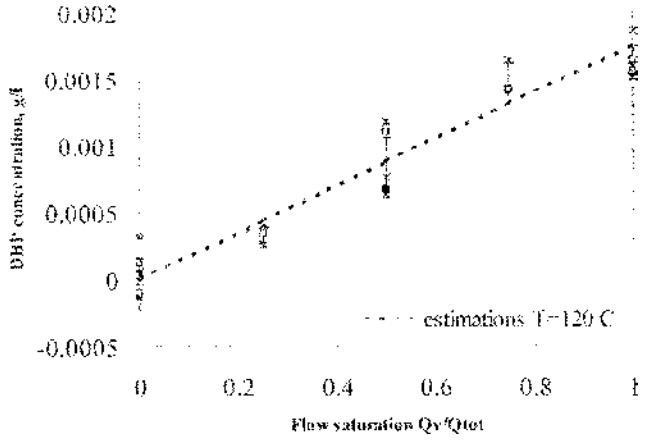

Figure 3. Dependence of the DBP vapor concentration in the outlet of the saturator chamber on the flow saturation ratio for saturator temperatures of 120°C. Dotted lines represent estimations based on saturated vapor pressure, and symbols are experimental values.

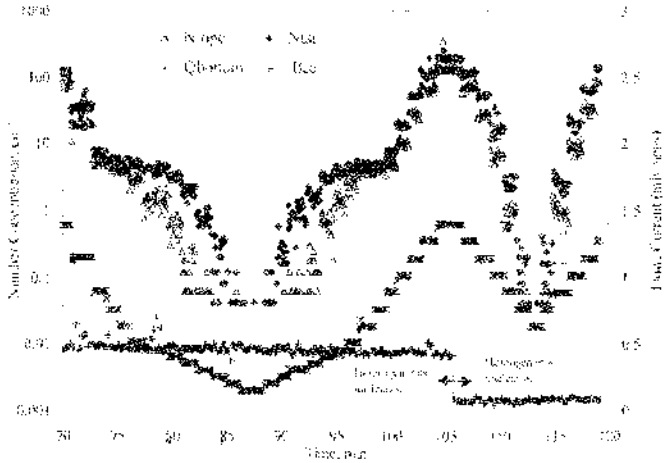

Figure 4. Variation of particle concentration measured by TSI CNC 3760 (N_{tsi}) and by PMS OPC (N_{opc}) in the supersaturation scanning experiment. Supersaturation was changed by means of DBP saturation flow (Q_{bottom}) in the presence of 1.7 nm particles ($t < 105$ min) and in the absence of particles. The presence of particles is indicated by FCE current (I_{fce}).

is gas constant (0.0821 atm*L/mol*K), and T is temperature of the saturator. Saturated vapor pressures $P_{sat}(T)$ were estimated with parameters as used by Okuyama et al. (1984) and were 18 and 24.7 Pa for saturation temperatures of 115 and 120°C, respectively. As can be seen in Figure 3, the dependence of DBP vapor concentration in the outlet of the saturator chamber is in good agreement with the calculated values. Measured vapor concentration values for other flow rates and temperatures are also in agreement with estimations.

Experiment and Data Reduction

All of the instruments used in the experiment were controlled by a single personal computer that allowed the synchronization of different devices and simplifying data collection of multiple variables in a dynamic situation. Typical experimental procedures consist of setting a working temperature for the TMCNC, setting parameters for particle generators, setting the desired nuclei size and composition, and scanning TMCNC supersaturation by changing the ratio of saturated/bypass flows in the vapor generator. During supersaturation scanning, all of the experimental variables were recorded. Figure 4 represents the typical variation of these variables during a supersaturation scanning experiment in the presence of 1.7 nm particles ($t < 105$ min) and in the absence of particles ($t > 105$ min). Variations in particle concentration were measured by TSI CNC 3760 (N_{tsi}) and by PMS OPC (N_{opc}) and are presented along with the variation of DBP saturation flow (Q_{bottom}) and FCE current (I_{fce}). The presence of particles is indicated by FCE current, which changes as DMA voltage is lowered to zero ($t = 105$ min). As can be seen in Figure 4, both counters give comparable values of particle concentration at higher values of Q_{bottom}, at lower values of Q_{bottom} the N_{tsi} and N_{opc} data differ due to the different detection limits. The particle number concentration changes sharply with changes in supersaturation in the absence of initial nuclei indicating homogeneous nucleation. When particles are present, there are two "waves" of concentration increase related to the start of heterogeneous and homogeneous nucleation. Similar behavior is observed on increasing and decreasing the supersaturation, indicating the monotonic relation between the flow ratio in the vapor generator and the resulting supersaturation.

The number concentration of particles detected by the different sensors (TSI CNC 3760 (N_{tsi}, $d > 14$ nm), PMS OPC (N_{opc}, $d > 0.5$ μm), and LAS-X (N_{las} 1–2)) at different DBP vapor pressures is presented in Figure 5. For the LAS-X data, two size ranges are presented with detection limits of 0.3 μm and 0.17 μm, respectively. The FCE current (I_{fce}) represents the initial concentration of nuclei that remains constant during the experiment. There are significant differences in the data from sensors at vapor pressure values below 0.93 Pa. The OPC and LAS-1 data are significantly lower than the TSI points. The grown particle size decreases as the vapor pressure decreases and causes these differences because the particles then become smaller than the detection limit of OPC. At the end of the pressure scanning range, the LAS-2 points become lower than the TSI value, indicating the shift of grown particle size below the 170 nm range. The good agreement between the TSI CNC and LAS-X data at higher values of vapor pressure indicates that the size distribution of grown particles is stable and the measured data are valid.

The size distributions of grown particles are shown in Figure 6 for both heterogeneous nucleation and homogeneous nucleation. Figure 6a shows the size distributions of heterogeneous nucleation of DBP, at three initial vapor pressures, on NaCl particles with a mobility equivalent size of 1.7 nm. As vapor pressure

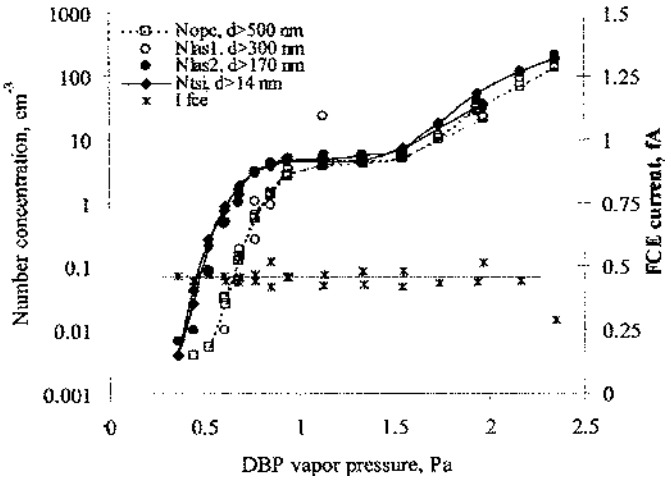

Figure 5. Number concentration of particles detected by different sensors: TSI CNC 3760 (N_{tsi}), PMS OPC (N_{opc}), and LAS-X (N_{las} 1–2) at different DBP vapor pressures. For LAS-X data, two size ranges are presented with detection limits of 0.3 mm and 0.17 mm, respectively. The FCE current (I_{fce}) represents the initial concentration of nuclei.

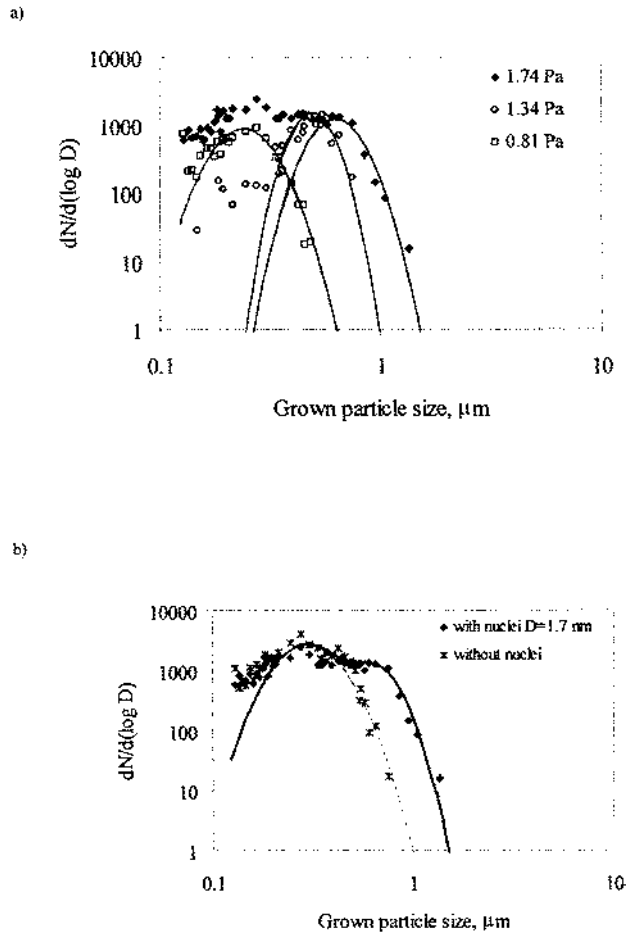

Figure 6. (a) Size distribution of grown particles measured by LAS-X at different DBP vapor pressures. NaCl particles of 1.7 nm were used as nuclei. (b) Size distribution of grown particles for homogeneous and heterogeneous nucleation at DBP vapor pressure of 1.73 Pa. Points in both figures are experimental data; lines are lognormal approximation.

increases, the modal size of grown particles shifts to the right. At a pressure of 0.80 Pa, the lognormal size distribution fits well with the experimental results. At high pressure, however, a small tail can be seen at the lower size end. This tail becomes predominant for even higher pressure. Apparently, homogeneous nucleation of DBP at this value of vapor pressure overtakes heterogeneous nucleation. This observation is confirmed by data presented in Figure 6b, where size distributions are presented for homogeneous and for heterogeneous nucleation at the same initial DBP vapor pressure of 1.73 Pa. The filled symbols are data for 1.7 nm NaCl nuclei, while the open symbols are data obtained from homogeneous nucleation of DBP vapor in the absence of NaCl nuclei. The solid line is the superposition of two lognormal size distributions: one corresponds to heterogeneous nucleation of 1.7 nm nuclei and the other corresponds to homogeneous nucleation of DBP vapor. The solid line fits well the data for NaCl nuclei, indicating the simultaneous occurrence of homogeneous nucleation and heterogeneous nucleation.

The data presented in Figure 5 shows a typical example of the transition from heterogeneous to homogeneous nucleation. The effect of the initial nuclei sizes on this transition is presented in Figure 7 and shows the dependence of the particle concentration on DBP vapor pressure for different initial nucleus size and for homogeneous nucleation. The FCE current for each particle size is also presented. In the case of homogeneous nucleation, the DMA voltage was turned to zero and FCE current was at background levels (see Figure 5, $t > 105$ min). Both of the heterogeneous nucleation curves in Figure 7 have similar patterns. As the vapor concentration increases, the number of detected particles starts to increase. For particles of initial DMA sizes of 1.4 and 2 nm, the increasing concentration reaches a "plateau" before starting to increase again. The second increase of particle concentration is caused by homogeneous nucleation of DBP vapor, as indicated by the curve for homogeneous nucleation in Figure 7. For particles of 1.4 nm, the concentration curve changes slope as the DBP vapor concentration reaches the homogeneous nucleation range.

Simultaneous measurements of FCE current and particle concentration detected by CNC allow for comparison between these two concentrations in order to determine the detection efficiency of the CNC. The FCE current is recalculated to particle concentration, assuming each particle carries a single negative charge (the fraction of multiple charged particles for a particle size below 20 nm is negligible). The concentration is reduced by the dilution factor in the outlet of the DMA system (see Figure 2) and in the CNC. Diffusion losses in the tube connecting the DMA system and CNC inlet are estimated and taken into account. CNC/FCE ratios measured for different particle sizes at

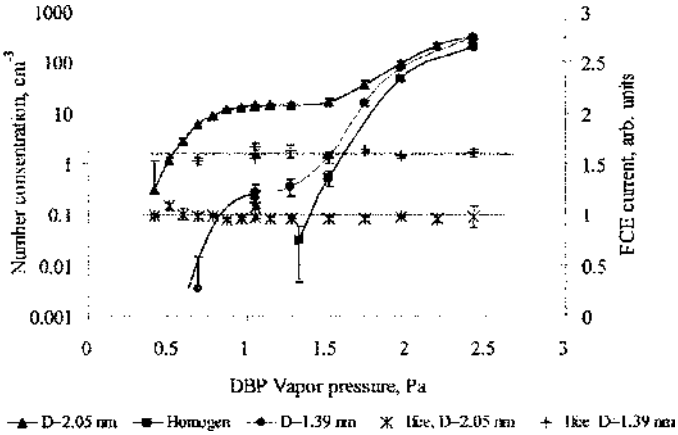

Figure 7. The dependence of particle concentration on DBP vapor pressure for different initial nucleus size and for homogeneous nucleation. The FCE current for each particle size is also presented.

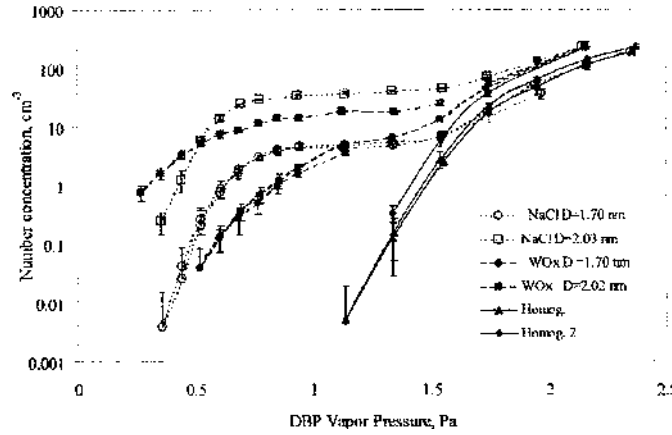

Figure 9. The dependence of particle concentration on DBP vapor pressure for different initial nuclei sizes and compositions and for homogeneous nucleation. The results for 1.7 nm and for homogeneous nucleation (Homog.) consist of two sets of data obtained by decreasing and increasing the vapor pressure.

different DBP vapor pressures are presented in Figure 8. Changing the DBP vapor pressure within the operational limits of the system does not influence the detection of particles >2.6 nm to any significant degree. As shown in the previous figures, homogeneous nucleation prevails over heterogeneous nucleation at DBP pressures above 1.73 Pa, giving unreasonable values of the CNC/FCE ratio that exceed 1. For smaller particles, the detection efficiency shows a strong dependence on DBP vapor pressure.

Results and Discussion

Experiments were performed with two types of nuclei. WO_x and NaCl particles were generated simultaneously and were used in equal experimental conditions. The dependence of detected particle concentration on DBP vapor pressure for different initial nuclei sizes and compositions is presented in Figure 9. The results for 1.7 nm and for homogeneous nucleation (Homog.) consist of two sets of data obtained by decreasing and increasing the DBP vapor pressure. The transition from heterogeneous nucleation to homogeneous nucleation is very similar for both types of nuclei. Particle concentration increases with increasing vapor pressure, reaches a "plateau," and converges to the curve for homogeneous nucleation.

There are also differences between these two types of nuclei. These differences are more pronounced in Figure 10. In this figure, the dependence of the detection efficiency (CNC/FCE ratio) on vapor pressure for different sizes and composition of nuclei is presented. The impact of homogeneous nucleation caused by the increase in particle concentration at DBP pressures above 1.60 Pa (see Figure 9) has been subtracted. The major difference in data for WO_x and NaCl is in the slope of the rising part of

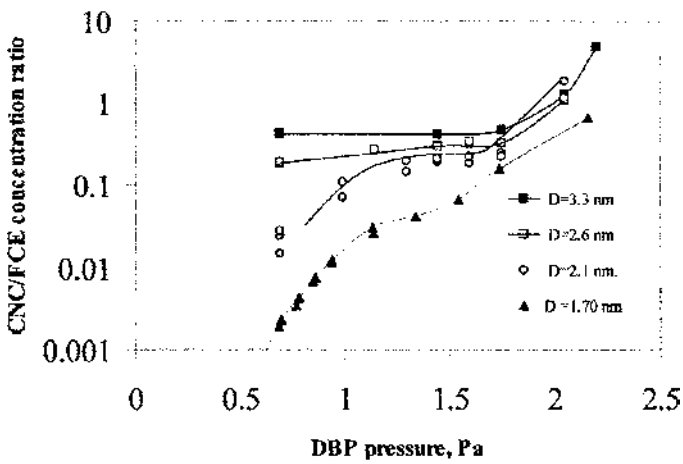

Figure 8. Dependence of detection efficiency (CNC/FCE concentration ratio) on DBP vapor pressure for different sizes of tungsten oxide (WO_x) nuclei.

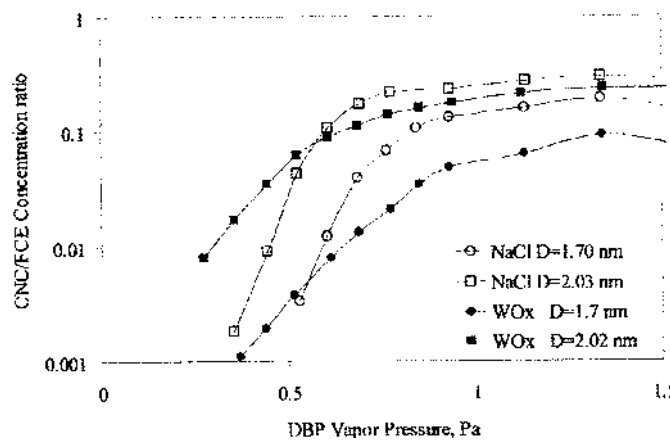

Figure 10. Dependence of detection efficiency (CNC/FCE ratio) on vapor pressure for different sizes and compositions of nuclei.

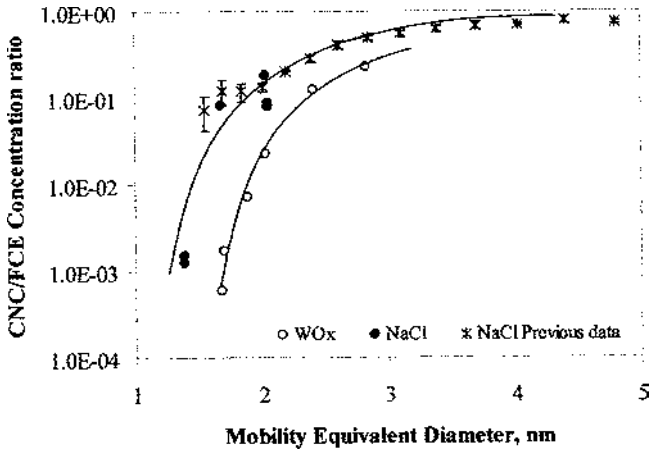

Figure 11. The detection efficiency of TMCNC (CNC/FCE concentration ratio) for different nuclei sizes and compositions. Recent data for NaCl and WO_x is compared with NaCl data at a flow rate of 1 l/min (previous data), which were obtained during the Vienna Workshop of CNC's Intercomparison (Ankilov et al. 1994).

the detection efficiency curves. The curves for different particle sizes of the same substance are essentially parallel. When curves are reaching a "plateau," the detection efficiency also varies with particle size and substance. The dependence of detection efficiency on particle size for different compositions of nuclei is presented in Figure 11 (data presented is for fixed value of vapor pressure of 1.33 Pa). The data points for the sample flow rates of 1 l/min were obtained during the International Workshop on comparison of CNC instruments at Vienna University (Ankilov et al. 1994) and are presented here for comparison with recent measurements at a sample flow rate of 2 l/min. The NaCl data points for different flow rates converge to a single curve. At the same time, the CNC detection efficiency for WO_x particles is substantially lower than that for NaCl particles for DBP vapor pressure values of 1.33 Pa. As observed in Figure 10, the situation reverses at lower DBP pressures where WO_x particles have higher detection efficiency. This fact cannot be explained with available theories. Further experimental and theoretical research on this subject is required.

CONCLUSIONS

A novel CNC was developed that is capable of scanning a range of supersaturation values via turbulent mixing of two flows, one with nuclei and the other with DBP vapor. The vapor pressure of DBP was controlled by splitting the vapor generator flow and saturating only a predetermined part of the flow while the total flow and temperature remained constant. This approach allows for the changing of the initial DBP vapor pressure while keeping the flow structure and the temperature field unchanged. The DBP concentration in the outlet of the vapor generator was measured experimentally for different ratios of saturated and bypass flows and found to be close to the estimated values.

The transition from heterogeneous nucleation to homogeneous nucleation was investigated using the scanning CNC. With an increase of DBP vapor pressure, the concentration of enlarged particles increased and reached a plateau. At higher values of DBP pressure and correspondingly higher supersaturation values, homogeneous nucleation prevails and the number concentration of particles follows the curve typical for homogeneous nucleation recorded in the absence of nuclei. Nuclei with different mobility diameters were activated at different values of vapor pressure. The differences between homogeneous and heterogeneous nucleation were correlated with nucleus mobility sizes.

Factors affecting heterogeneous nucleation for different types of nuclei were investigated using the scanning CNC. Experimental results are presented for NaCl and WO_x particles at various DBP vapor pressures. There are significant differences in the slopes of particle activation curves for NaCl and WO_x particles. The reasons for such differences are a subject for continuing research.

ACKNOWLEDGMENT

This work was supported by the US Environmental Protection Agency under grant R826654.

REFERENCES

Abramovich, G. N. (1963). *The Theory of Turbulent Jets*, MIT Press, Cambrige, MA, p. 633.

Adachi, M., Okuyama, K., and Seinfeld, J. H., (1992). Experimental studies of ion-induced nucleation. *J. Aerosol Sci.* 23, 4:327–337.

Agarwal, J. K., and Sem, G. J. (1980). Continuous Flow, Single-Particle Counting Condensation Nucleus Counter, *J. Aerosol Sci.* 11:343–357.

Ahn, K. H., and Liu, B. (1990). Particle Activation and Droplet Growth Process in Condensation Nucleus Counter-I. Theoretical Background, *J. Aerosol Sci.* 21:263–276.

Ankilov, A., Baklanov, A., Colhoun, M., Enderle, K.-H., Filipovicova, D., Gras, J., Julanov, Y., Lindner, A., Lushnikov, A., Majerowicz, A., Mavliev, R., McGovern, F., Mirme, A., O'Connor, T., Podzimek, J., Preining, O., Reischl, G., Rudolf, R., Sem, G., Szymanski, W., Tamm, E., Wagner, P., Winklmayr, W., and Zagainov, V. (1994). Sensitivity of Various Aerosol Counting Methods for Different Particle Size and Compositions: Results of Vienna Workshop 1993. *Proc. of Fourth International Aerosol Conference*, edited by R. Flagan. Los Angeles, CA, pp. 375–376.

Ankilov, A., Baklanov, A., Eremenko, S., Mavliev, R., Reischl, G., and Majerowicz, A. (1991). Comparison of the Novosibirsk Diffusion Battery with the Vienna Electromobility Spectrometer, *J. Aerosol Sci.* 22:s325–328.

Fissan, H. D., Stratmann, F., Buscher, P., Neumann, S., Pui, D., and Chen, D. (1996). Experimental Comparison of Four Differential Mobility Analyzers for Nanometer Aerosol Measurement, *Aerosol Sci. Technol.* 24:1–13.

Fletcher, N. (1969). *The Physics of Rainclouds*, Cambrige University Press, London.

Helsper, C., and Niessner, R. (1985). On the Influence of the Vapour Substance on the Behavior of an Expansion-Type Condensation Nucleus Counter, *J. Aerosol Sci.* 16:457–461.

Kesten, J., Reineking, A., and Porstendörfer, J. (1991). Calibration of a TSI Model 3025 Ultrafine Condensational Particle Counter, *Aerosol Sci. Technol.* 15:107–111.

Kim, T. O., Ishida, T., Adachi, M., Okuyama, K., and Seinfeld, J. H. (1998). Nanometer-Sized Particle Formation from NH3/SO2/H2O/Air Mixtures by Ionizing Irradiation, *Aerosol Sci. Technol.* 29:112–125.

Kogan, Y., and Burnashova, Z. (1960). Size Magnification and Measurement of Condensation Nuclei in the Continuous Flow, *J. Phys. Chem.* 34:2630–2639 (in Russian).

Kousaka, Y. (1993). *Mixing Type CNC and its Applications*. Report on International Conference on Aerosol Science and Technology. Taichung, Taiwan, R.O.C.

Kousaka, Y., Okuyama, K., and Niida, T. (1984). Size-Supersaturation Relationship in Activation of Ultrafine Aerosol Particles. In *Aerosols*, edited by B. Liu, D. Pui, and H. Fissan. Elsevier, New York, p. 51.

Madeline, G., and Metayer, Y. (1980). Technical Note, *J. Aerosol Sci.* 11:358.

Makela, J. M., Mavliev, R., and Jokinen, V. (1996). On the Detection Efficiency of Ultrafine Condensation Particle Counter (UCPC, TSI Model 3025) Below 3 nm. In *Nucleation and Atmospheric Aerosols*, edited by M. Kulmala and P. Wagner. Elsiver Publishing, pp. 643–646.

Mavliev, R., and Wang, H.-C. (2000). Design and Performance Characteristics of a Turbulent Mixing Condensation Nuclei Counter, *J. Aerosol Sci.*, in press.

McDermont, W. T., Ockovic, R. C., and Stolzenburg, M. R. (1991). Counting Efficiency of an Improved 30-A Condensation Nucleus Counter, *Aerosol Sci. Technol.* 14:278–287.

Okuyama, K., Kousaka, Y., and Motouchi, T. (1984). Condensation Growth of Ultrafine Aerosol Particles in a New Particle Size Magnifier, *Aerosol Sci. Technol.* 3:353–366.

Porstendörfer, J., Scheibel, H., Pohl, F., Preining, O., Reischl, G., and Wagner, P. (1985). Heterogeneous Nucleation of Water Vapor on Monodispersed Ag and NaCl Particles with Diameters between 6 and 16 nm, *Aerosol Sci. Technol.* 4:65–79.

Rebours, A., Bouland, D., and Renoux, A. (1996). Recent Advances in Nanoparticle Size Measurement, *J. Aerosol Sci.* 27:1227–1242.

Reischl, G. P., Makela, J. M., and Necid, J. (1997). Performance of Vienna Type Differential Mobility Analyzer at 1.2–20 Nanometer, *Aerosol Sci. Technol.* 27:651–672.

Rossel-Liompart, F., Losceratales, I., Bingham, D., and Fernandez de la Mora, J. (1996). Sizing Nanoparticles and Ions with a Short Differential Mobility Analyzer, *J. Aerosol Sci.* 27:695–720.

Saros, M. T., Weber, R. J., Marti, J. J., and McMurry, P. H. (1996). Ultrafine Aerosol Measurement Using a Condensation Nucleus Counter with Pulse Height Analysis, *Aerosol Sci. Technol.* 25:200–213.

Scheibel, H., and Porstendörfer, J. (1986). Counting Efficiency and Detection Limit of Condensation Nuclei Counters for Submicrometer Aerosols, *J. Colloid Interface Sci.* 109:261–274.

Stolzenburg, M. (1988). *An Ultrafine Size Distribution Measuring System*, Ph.D. thesis, University of Minnesota, Minneapolis, MN.

Stolzenburg, M. R., and McMurry, P. H. (1991). An Ultrafine Aerosol Condensation Nucleus Counter, *Aerosol Sci. Technol.* 14:48–65.

Willeke, K., and Baron, P., eds. (1993). *Aerosol Measurement: Principles, Techniques and Applications*, Van Nostrand Reinhold, New York.